Science Press

ARTICLE

Effect of SiO$_2$ Nanoparticles/Silicate on Characteristics of Micro-arc Oxidation Coating Formed on TC4 Alloy

Sun Fengyu[1],   Yang Zhao[1],   Hu Jie[2],   Gong Yunbai[1],   Wang Ping[1],   Luo Qiming[1], Zhu Manlan[1]

[1] School of New Energy and Materials, Southwest Petroleum University, Chengdu 610500, China; [2] State Key Laboratory of Low-carbon Smart Coal-fired Power Generation and Ultra-clean Emission, Nanjing 210046, China

Abstract: TC4 micro-arc oxidation (MAO) coatings were prepared by adding SiO$_2$ nanoparticles or sodium silicate to the sodium meta-aluminate-based electrolyte. The effect of additives was investigated by XRD, SEM, EDS, electrochemical and wear tests. The results show that additives can considerably accelerate the formation of MAO coatings. The coatings are mostly composed of rutile and anatase TiO$_2$, α-Al$_2$O$_3$, γ-Al$_2$O$_3$, Al$_2$TiO$_5$ and SiO$_2$. Sodium silicate and SiO$_2$ nanoparticles added to the coating can effectively reduce the size of micropores and increase its thickness, whereas SiO$_2$ nanoparticles with superior physical properties can be directly deposited at the discharge channel, significantly increasing the coating's resistance to wear and corrosion. The coating with SiO$_2$ nanoparticles exhibits the best overall performance, with the lowest corrosion rate and average friction coefficient of 4.095×10^{-5} mm/a and 0.30, respectively.

Key words: micro-arc oxidation; TC4 alloy; coatings; corrosion; wear

TC4, widely utilized in aerospace, oil drilling, and biomedical sciences, offers higher specific strength and corrosion resistance than other candidate materials such as ferritic stainless steels, Ni-based, aluminum-based, and magnesium-based alloys[1–3]. It is recognized that the natural oxidation layer is primarily responsible for the exceptional properties of titanium and its alloys, which has high hardness, good chemical stability and corrosion resistance, but is too thin to exist after continuous wear and tear, resulting in direct exposure of the matrix to corrosive medium[4–5], which restricts the development of titanium industry.

Micro arc oxidation (MAO) prepares ceramic coatings by plasma discharge on valve metal substrates including titanium, magnesium and aluminum alloys, achieving improvement of corrosion resistance, wear resistance and other characteristic[6–8]. Since high hardness components like Al$_2$O$_3$ and Al$_2$TiO$_5$ are formed in the coating, the aluminate-based titanium alloy coating has a potentially great wear resistance[9–10]. The ceramic coatings, however, have a non-uniform thickness because of the instability of NaAlO$_2$, which

actually affects the antiwear and anticorrosion ability[11]. It has been reported that treatment time, electrical parameters, electrolyte and substrate are key factors influencing the characteristic of MAO coatings[12–14], in which the electrolyte has attached much interest because it can be easily altered by adding different additives, thus affecting the formation of coating or incorporating components of additives into the coating[15–16]. Zhong et al[17] incorporated Ga ions (amorphous Ga$_2$O$_3$ and GaPO$_4$) into the MAO coatings, and improved the antibacterial and anticorrosion ability. Nikoomanzari et al[18] used the ZrO$_2$ nanoparticles to improve the morphology, wettability, antibacterial and corrosion behavior of MAO coatings. Wang et al[19] studied the influence of nano TiO$_2$ particles on the MAO process, and found that the efficiency and compactness of the coating increase, as well as the hardness of coating. It is known that the SiO$_2$ is widely used in ceramic fields to enhance toughness and anti-abrasive property[20–21]. Meanwhile, these additions in the electrolyte can accelerate the growth rate of the coatings[8, 22–23]. After adding SiO$_2$ nanoparticles or silicate, the coating may be

doped with amorphous SiO_2 by plasma discharge, optimizing the coating structure and improving corrosion and wear resistance.

In this work, TC4 alloy was treated by MAO with silicate and SiO_2 nanoparticles added in aluminate solution. The microstructure, composition phase, corrosion and wear resistance of coating were characterized.

1 Experiment

TC4 alloy specimens (15 mm×15 mm×3 mm) were used as the matrix material in this experiment. The sample surface oxidation layer was removed with 400#, 800#, 1200# and 1500# sandpaper, then ultrasonically cleaned with ethanol for 10 min and finally dried by a hairdryer after being cleaned with deionized water. Composition of different electrolytes is listed in Table 1. The conductivity and pH values of several electrolytes were tested by a pen-style pH meter (PH-10,

China) and a conductivity meter (DDS-307, China) and the findings are displayed in Table 2. The MAO coatings prepared in different electrolytes were marked as 1#, 2# and 3#. The MAO electrical parameters are 5 A/dm², 600 Hz, 40% duty cycle, the experimental time was 30 min, and the temperature was 25±5 °C.

The surface and cross-section were characterized by scanning electron microscope (SEM, ZEISS EVO MA15, Germany) with X-ray energy dispersive spectrometer (EDS, OXFORD, America). The main phase composition was analyzed by X-ray diffractometer (XRD, DX-2700B, China), with the following parameters: voltage of 40 kV, current of 30 mA, scanning angle 2θ of $10° – 80°$, scanning progression angle of 0.05°, scanning step time of 0.2 s, and Cu-targeted Kα radiation source. The hardness was measured by digital microhardness tester (HXD-2000TM/LCD, China), the thickness was measured by eddy current thickness gauge

Table 1 Electrolyte composition of MAO coatings

Sample	System	Electrolyte
1#	Aluminate	12 g/L $NaAlO_2$
2#	Aluminate-silicate	12 g/L $NaAlO_2$-4 g/L Na_2SiO_3
3#	Aluminate-SiO_2 nanoparticles	12 g/L $NaAlO_2$-2 g/L SiO_2 nanoparticles

(TT230, China), and the average of 5 points for both thickness and hardness measurements was taken as the final results. The polarization curve and AC impedance were tested by electrochemical workstation (Gamry Reference 3000, America) in the frequency range of $10^5 – 10^{-1}$ Hz with an opencircuit potential of ±0.25 V. Calomel electrode was used as the reference electrode, with the platinum electrode as the auxiliary electrode and the samples as the working electrode. The corrosion solution was 3.5wt% NaCl solution, and samples were coated with epoxy resin before being placed in a 1 cm² test area. The reciprocating friction test used a multifunctional material testing machine (MFT-4000, China), in which the friction partner was GCr15 ball, and friction length was 5 mm. The experiment lasted for 30 min under the loading force of 2 N and the morphology of the wear marks was studied by SEM finally.

2 Results and Discussion

2.1 Influence of electrolytes on MAO voltage

Fig. 1 depicts the voltage curves of three coatings during MAO process, and Fig.2 depicts their breakdown and ultimate voltage. Compared to electrolytes 1# and 3# with a conductivity of 14.6, due to the addition of silicates, electrolyte 2# has a higher conductivity of 16.3, promoting metal surface passivation to form a thin dielectric insulating layer[24] and

Table 2 Electrical conductivity and pH value of electrolyte

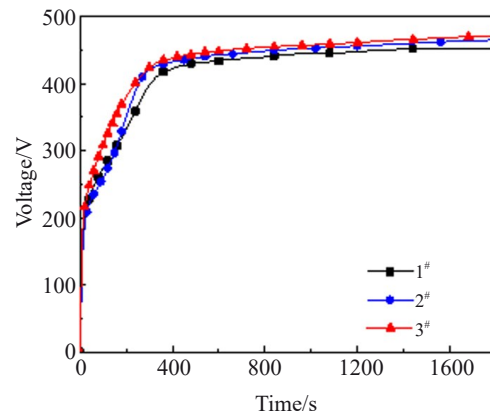| Sample	1#	2#	3#
Electrical conductivity	14.6	16.3	14.6
pH value	13.8	14.2	13.8

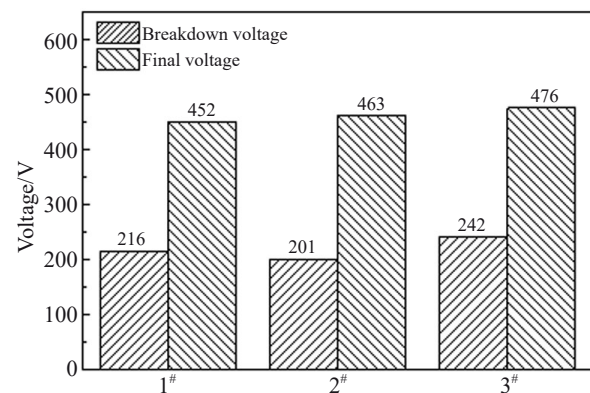Fig.1 Voltage curves of three coatings

Fig.2 Breakdown and final voltages of three coatings

resulting in the oxidation to enter the spark discharge stage at a relatively low breakdown voltage. Moreover, SiO_3^{2-} has a strong adsorption capacity, and is easily adsorbed on the surface of titanium substrate to form impurity discharge center during the oxidation process[25]. While the SiO_2 nanoparticles will be enriched on the surface of anode under electric field and in mechanical stirring because these particles get weak negatively charged under the hydration, increasing the surface passivation resistance[26]. Thus, the electrolyte with nano-particles has a higher breakdown voltage. Furthermore, nanoparticles can become heterogeneous nucleation center in the deposition stage[27]. In the constant current model, higher final voltage means a relative thicker and more compact coating generated on the matrix[28]. Both electrolyte additions have an impact on speeding oxidation deposition efficiency, resulting in enhanced coating structure.

2.2 Surface morphology and element distribution

Fig. 3 depicts the surface morphologies of three coatings. The surface shows a typical MAO porous structure with holes formed by the micro arc discharge due to the MAO principle[8]. On the coating surface, it mainly contains O, Ti and Al elements, as shown in EDS results (Table 3). Coating 3# shows more micropores and holes than coating 2#, which is attributed to violent micro arc discharge by higher final voltage, leaving some large pores. Since the micropores in coating 2# can be filled with electrolyte substrate, it exhibits a

distinct deposition trail on the surface. Coating 3# contains big nanoparticles that resemble SiO_2 nanoparticles (Fig.3e−3f). It is deduced that the nanoparticles in the surface pores are SiO_2, as research has shown that ceramic powders (such ZrO_2 and SiC) do not change form during the MAO process[29]. Additionally, it is evident (Fig.3e) that in some areas, particles fill the gaps left by the micro arc discharge, and EDS further confirms the presence of element Si in the MAO coating.

2.3 Surface phase composition

The main phase composition is shown in Fig.4. The micro-arc discharge converts the matrix and electrolyte into ions, which then create appropriate compounds, according to the MAO rule[8]. The main phases of the coatings are rutile TiO_2, anatase TiO_2, α-Al_2O_3, γ-Al_2O_3 and Al_2TiO_5, while SiO_2 is visible in the 2# and 3# coatings:

$$2H^+ + 2e^- \rightarrow H_2 \uparrow \tag{1}$$

$$4OH^- \rightarrow 2H_2O + O_2 + 4e^- \tag{2}$$

$$Ti \rightarrow Ti^{4+} + 4e^- \tag{3}$$

$$Ti^{4+} + 4OH^- \rightarrow TiO_2 + 2H_2O \tag{4}$$

$$AlO_2^- + 2H_2O \rightarrow Al(OH)_3 \tag{5}$$

$$2Al(OH)_3 \rightarrow Al_2O_3 + 3H_2O \tag{6}$$

$$Al_2O_3 + TiO_2 \rightarrow Al_2TiO_5 \tag{7}$$

$$Al(OH)_3(Amorphous) \xrightarrow{300\,°C} \gamma\text{-}Al_2O_3 \xrightarrow{800-1200\,°C} \alpha\text{-}Al_2O_3 \tag{8}$$

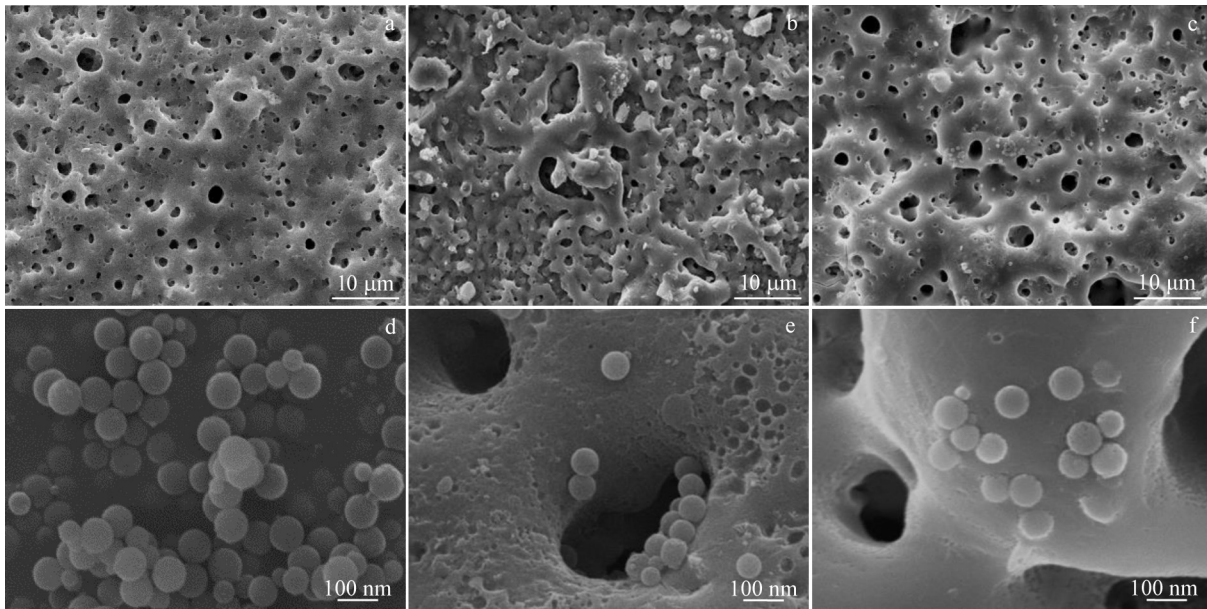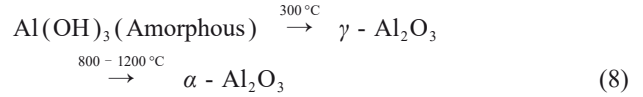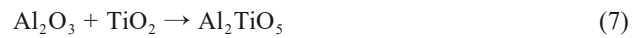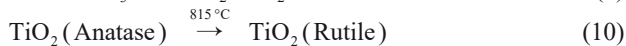Fig.3 Surface morphologies of coatings 1# (a), 2# (b), and 3#(c); shape of SiO_2 nanoparticles (d); magnified coating 3# (e−f)

$$2H^+ + SiO_3^{2-} \rightarrow SiO_2 + H_2O \tag{9}$$

$$TiO_2(Anatase) \xrightarrow{815\,°C} TiO_2(Rutile) \tag{10}$$

Due to increased energy input, the rise in oxidation voltage speeds up the transition of anatase TiO_2 to rutile TiO_2 and Al_2O_3 to α-Al_2O_3, γ-Al_2O_3 and Al_2TiO_5. The appearance of Ti peak in the XRD spectrum is detected by X-ray scanning in the porous structure of the coatings and the substrate.

Table 3 EDS results of MAO coatings

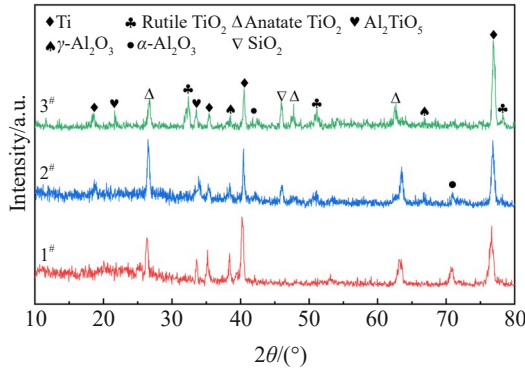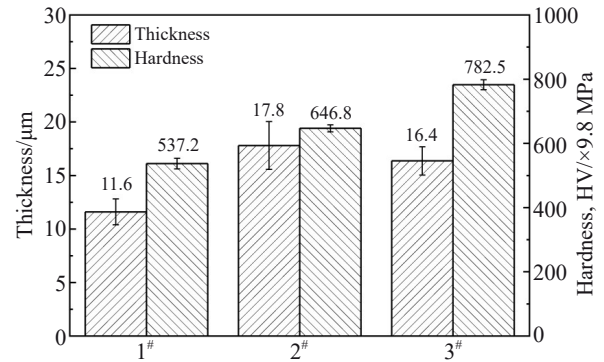| Sample	Ti	Al	O	Si
1#	17.25	23.69	59.06	0
2#	15.30	22.33	52.74	4.63
3#	16.73	24.76	53.57	4.94

Fig.4 XRD patterns of three coatings

Fig.5 Thickness and hardness of three coatings

2.4 Thickness and hardness

Fig. 5 displays the thickness and hardness of the MAO coatings, and Fig.6 shows the cross-section morphologies and EDS elements distribution. Compared to coating $1^{\#}$ with a thickness of 11.6 μm in single aluminate electrolyte (Fig.6a), coating $2^{\#}$ enters the MAO stage faster due to the addition of silicates in the electrolyte, resulting in a maximum coating thickness of 17.8 μm (Fig.6d). Because of the addition of SiO_2 in the electrolyte, higher reaction voltage increases the rate of coating formation, and the thickness of coating $3^{\#}$ is 16.4 μm (Fig.6h). Due to hard phase SiO_2, the hardness of coatings $2^{\#}$ and $3^{\#}$ is improved dramatically by 6338.64 and 7668.5 MPa, respectively, compared to that of coating $1^{\#}$ (5264.56 MPa).

The EDS results show that Si elements effectively penetrate coatings $2^{\#}$ and $3^{\#}$ (Fig.6g and 6k), and the distribution of the Ti element becomes more uniform, which is a sign of denser coating (Fig. 6b, 6e, and 6i). Compared to coating $2^{\#}$, Si element distribution in coating $3^{\#}$ matches O element distribution and is denser (Fig. 6j and 6k), implying that coating $3^{\#}$ can effectively block the discharge pores by filling them with SiO_2 nanoparticles, resulting in compact coating structure. Even though some pores in coating $2^{\#}$ shrank because of the new amorphous phase SiO_2, the breakdown rules of MAO keep porous. Coating $3^{\#}$ is the hardest due to its composition and structure.

2.5 Effect of electrolytes on corrosion resistance of MAO coatings

Electrochemical tests were used to study the corrosion resistance of coatings $1^{\#}$, $2^{\#}$, and $3^{\#}$ and substrate. Fig.7 shows corrosion potential (E_{corr}) and current density (I_{corr}), and the results of the Tafel fitting are shown in Table 4. MAO coatings show lower corrosion current density and rate than the
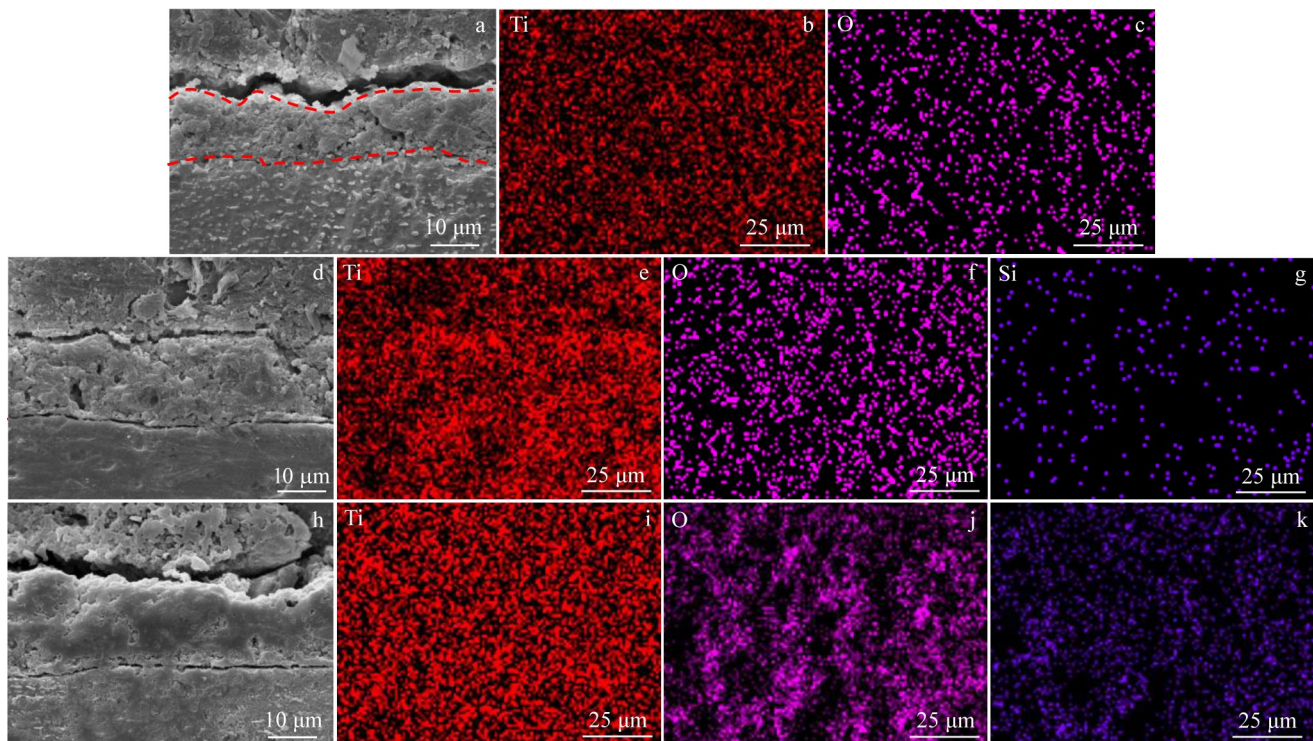
Fig.6 Cross-section morphologies and corresponding EDS element mappings of three coatings: (a–c) $1^{\#}$, (d–g) $2^{\#}$, and (h–k) $3^{\#}$
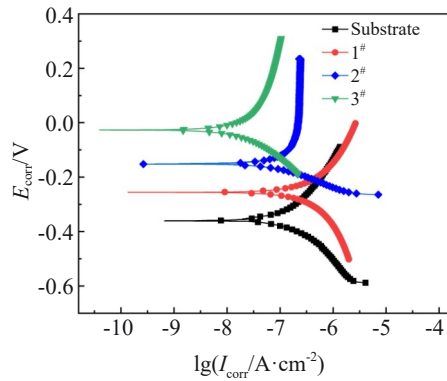
Fig.7   Polarization curves of substrate and three coatings

Table 4   Fitting results of potentiodynamic polarization curves of substrate and MAO coatings

Sample	E_{corr}/V	I_{corr}/A·cm^{-2}	Corrosion rate /mm·a^{-1}
Substrate	−0.3330	5.75×10^{-7}	6.570×10^{-3}
1$^{\#}$	−0.2560	3.72×10^{-7}	1.791×10^{-3}
2$^{\#}$	−0.1811	1.78×10^{-7}	6.617×10^{-4}
3$^{\#}$	−0.0294	4.94×10^{-8}	4.095×10^{-5}

substrate, indicating a higher level of corrosion resistance. Coatings' resistance is mostly controlled by their thickness and compactness, which has a direct impact on how well corrosion-causing substances penetrate the matrix. Compared to coating 1$^{\#}$, additives in electrolytes of coating 2$^{\#}$ and 3$^{\#}$ both modify the structure of coatings. In coating 2$^{\#}$, amorphous SiO$_2$ phase is generated to diminish the size and number of micropores. In coating 3$^{\#}$, SiO$_2$ nanoparticles directly fill micropores. These two coatings can successfully block the corrosion-causing agent. The corrosion currents of coatings 2$^{\#}$ and 3$^{\#}$ fall from 3.72×10^{-7} A/cm^2 to 1.78×10^{-7} and 4.94×10^{-8} A/cm^2, respectively. The corrosion rate also decreases from 1.791×10^{-3} mm/a to 6.617×10^{-4} and 4.095×10^{-5} mm/a, indicating that coating 3$^{\#}$ has the best corrosion resistance.

Fig. 8 shows the Nyquist diagram of substrate and coatings. Because the capacitive resistance arc represents the charge transfer resistance, a greater corrosion resistant coating typically has a bigger radius[30]. Both additions optimize the
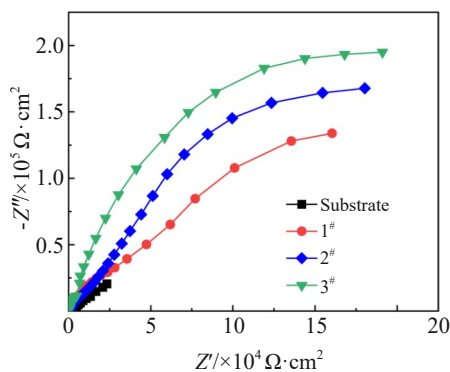

Fig.8   Nyquist plots of substrate and MAO coatings

coating corrosion resistance in accordance with the polarization curve, as evidenced by the broad radius of arc after the addition of silicate and SiO$_2$ nanoparticles. A coating with high impedance value in low-frequency region normally has excellent corrosion resistance[31]. In Fig. 9a, the impedance modulus (3$^{\#}$ >2$^{\#}$ >1$^{\#}$ >substrate) indicates that corrosion resistance of the substrate may be effectively enhanced by the coating, and the corrosion resistance increases with additives. The phase diagram of coatings, as shown in Fig. 9b, reveals an arc with two wave peaks and troughs, suggesting that the coating has double-layer membrane structure. Based on the aforementioned features of impedance plots and coatings, appropriate equivalent circuit models are used to analyze the impedance data, as shown in Fig. 10, in which R_1 is the solution resistance; R_2 and R_3 are resistance of sparse layer and dense layer, respectively; CPE$_1$-T and CPE$_2$-T are the capacitance of sparse layer and dense layer, respectively, and CPE$_1$-P and CPE$_2$-P are corresponding dispersion index[32]. The electrochemical impedance spectroscopy (EIS) results are shown in Table 5. R_3 is higher than R_2 since the MAO coating has a compact inner layer. R_3 and R_2 reach peak value in the 3$^{\#}$ sample because the SiO$_2$ nanoparticles serve as a barrier to the corrosive solution. In contrast, CPE$_1$-T and CPE$_2$-T values in 3$^{\#}$ sample are the lowest because the filling of nanoparticles in the coating makes it more difficult for the aggressive ions (Cl$^-$) to erode, resulting in a decrease in the inner layer's capacity to adsorb electrons. The antiseptic mechanism is shown in Fig. 11. CPE$_1$-P and CPE$_2$-P are influenced by the structure
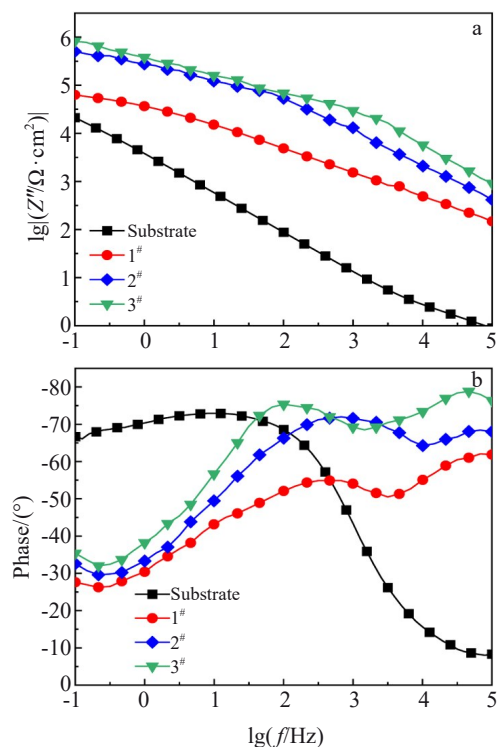

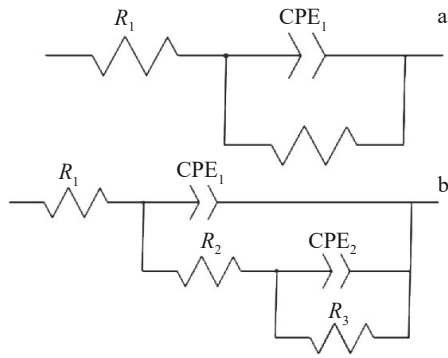Fig.9   Bode diagrams of substrate and MAO coatings: (a) impedance modulus; (b) phase angle

Fig.10 Equivalent circuit diagrams of EIS: (a) substrate; (b) MAO coatings

of the coating, i. e., denser coating has a higher CPE value. After adding additives, CPE_1-P increases from 0.64 to 0.88, and CPE_2-P increases from 0.70 to 0.93.

2.6 Effect of electrolytes on wear resistance of MAO coating

Fig. 12 depicts the coefficient of friction (COF) of three coatings in reciprocating friction experiments, and Table 6 shows the average COF. The results reveal significant changes in COF of coating 1[#], with an average value of 0.78, and visible increase in COF after 1200 s (Fig. 12), indicating that coating 1[#] has broken down. On the contrary, the COF of 2[#] and 3[#] coatings remain steady, with average values of 0.42 and 0.30, respectively, owing mostly to reduced surface roughness and improved coating structure uniformity. Meanwhile, the

Table 5 EIS fitting results of substrate and MAO coatings

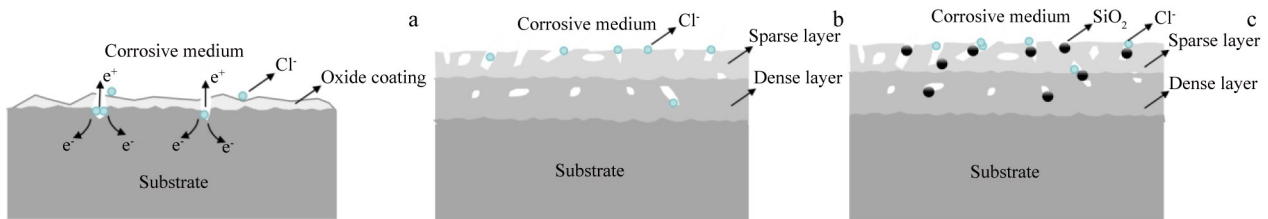| Sample	$R_1/\Omega\cdot cm^2$	CPE_1-T/$\Omega^{-1}\cdot cm^2\cdot s^{-p}$	CPE_1-P	$R_2/\Omega\cdot cm^2$	CPE_2-T/$\Omega^{-1}\cdot cm^2\cdot s^{-p}$	CPE_2-P	R_3
Substrate	6.916	9.45×10^{-5}	0.59	1.24×10^3			
1[#]	43.210	2.26×10^{-6}	0.64	2.37×10^3	5.81×10^{-7}	0.70	1.52×10^4
2[#]	35.640	6.73×10^{-6}	0.74	5.81×10^3	1.52×10^{-7}	0.82	4.69×10^5
3[#]	53.760	1.26×10^{-7}	0.88	2.83×10^4	2.13×10^{-8}	0.93	1.58×10^6

Fig.11 Diagrams of antiseptic mechanism: (a) substrate, (b) 1[#] and 2[#] coatings, and (c) 3[#] coating
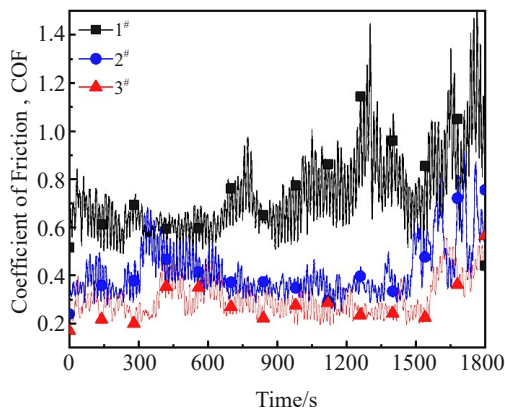

Fig.12 COF of three coatings at different time in reciprocating friction experiments

new tough phase SiO_2 in the coating can disperse some stresses to improve wear resistance. Fig. 13 shows morphologies of the wear marks after friction tests. The addition of additives causes the breadth of wear marks to shrink. Coating 1[#] in Fig. 13a–13c displays a wide, deep wear

groove, and some areas have significant destruction, which is because the rough coating increases the contact between hard phases and friction pair, resulting in increase in COF, severe wear and wider wear scar. In Fig. 13d–13i, the wear marks of 2[#] and 3[#] coatings are relatively narrow, indicating that the additives optimize the coatings' wear resistance by improving the density of coatings. Meanwhile, the SiO_2 phase in coatings exerts a lubricating effect on the friction pair during wear, lowering the wear degree of coatings. Due to high strength, hardness and dispersibility of SiO_2 nanoparticles on the surface of the coating, the best wear resistance of coating 3[#] is demonstrated by the smallest wear mark and the lowest average COF (0.30).

Table 6 Average COF of three coatings

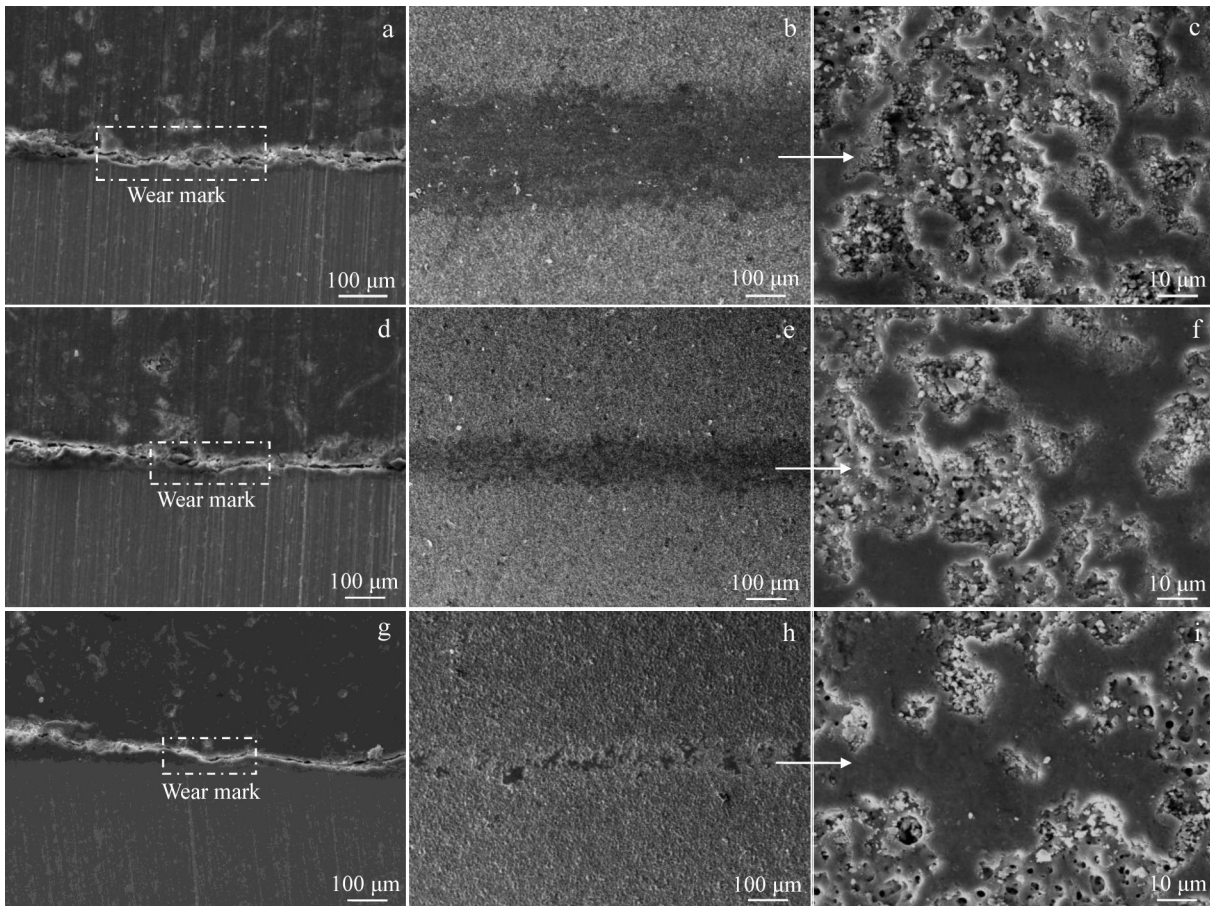| Sample	Average COF
1[#]	0.78
2[#]	0.42
3[#]	0.30

Fig.13 Cross-sectional morphologies and surface morphologies of wear marks of MAO coatings: (a–c) 1#, (d–f) 2#, and (g–i) 3#

3 Conclusions

1) The MAO coating on TC4 alloy in electrolytes with silicate or SiO$_2$ nanoparticles added remains porous structure due to MAO principle. Additives boost the transit efficiency of ions in the electrolyte, promoting coating formation. During the oxidation process, SiO$_3^{2-}$ in the silicate is adsorbed on the surface of titanium substrate to form impurity discharge center. While the SiO$_2$ nanoparticles become heterogeneous nucleation center in the deposition stage.

2) MAO coatings can significantly improve the corrosion resistance of the substrate, whereas both additions can enhance the corrosion resistance of the coatings. In the aluminate-silicate system, silicates enhance the conductivity of the solution, resulting in more complete reactions, faster coating formation rate, increased coating thickness and density, and improved corrosion resistance. In the aluminate-SiO$_2$ system, SiO$_2$ nanoparticles are adsorbed on coatings, increasing oxidation voltage and supplying energy for coating, while filling of micropores by SiO$_2$ significantly increases density and corrosion resistance.

3) MAO coating doped with SiO$_2$ nanoparticles demonstrates the best wear resistance thanks to the strength and dispersity of SiO$_2$ nanoparticles, with an average COF of 0.30.

References

1 Williams J C, Banerjee D. *Acta Materialia*[J], 2013, 61(3): 844

2 Wang Dong, Zhang Xiaojing, Dai Hongyuan *et al*. *Materials China*[J], 2024, 43(10): 924 (in Chinese)

3 Zhao Feng, Wang Xiao, Guo Shuxiang. *Materials China*[J], 2024, 43(11): 1030 (in Chinese)

4 Hu Bo, Jiang Yingxin, Liu Bin *et al*. *Titanium Industry Progress*[J], 2023, 40(6): 31 (in Chinese)

5 Ma Jiangnan, Yi Zhulin, Zhang Wenli *et al*. *Titanium Industry Progress*[J], 2024, 41(2): 24 (in Chinese)

6 Ren L, Wang T, Chen Z *et al. Medziagotyra*[J], 2019, 25(3): 270

7 Liu Yanming, Jia Xinlu, Zhang Yicai *et al*. *Materials China*[J], 2023, 42(9): 699 (in Chinese)

8 Wu T, Blawert C, Serdechnova M *et al. Applied Surface Science*[J], 2022, 595: 153523

9 He J Y, Wu X Q, Xie F Q *et al. Rare Metal Materials and Engineering*[J], 2023, 52(7): 2424

10 Molaei M, Fattah-Alhosseini A, Gashti S O. *Metallurgical and Materials Transactions A: Physical Metallurgy and Materials Science*[J], 2018, 49(1): 368

11 Liu F, Shimizu T. *Journal of the Ceramic Society of Japan*[J], 2010, 118(1374): 113

12 Wang P, Gong Z Y, Hu J *et al. Surface Engineering*[J], 2019, 35(7): 627

13 Duan Y F, Liu J W, Wang P. *Surface Engineering*[J], 2022, 38(4): 440

14 Lan X Y, Wang P, Gong Z Y *et al. Rare Metal Materials and Engineering*[J], 2024, 53(4): 954

15 Wang X J, Wang P, Liu Y *et al. Rare Metal Materials and Engineering*[J], 2023, 52(10): 3452

16 Ji P F, Lu K, Chen W D *et al. Rare Metal Materials and Engineering*[J], 2023, 52(5): 1583

17 Zhong S, Li G Q, Zhang S F *et al. Materials Chemistry and Physics*[J], 2022, 282: 125923

18 Nikoomanzari E, Fattah-alhosseini A, Alamoti M R P *et al. Ceramics International*[J], 2020, 46(9): 13114

19 Wang P, Wu T, Li J *et al. Rare Metal Materials and Engineering*[J], 2017, 46(2): 479

20 Tekeli S, Boyacıoğlu T, Güral A. *Ceramics International*[J], 2009, 34(8): 1959

21 Zhao T, Li A, Qin Y *et al. Journal of Non-Crystalline Solids*[J], 2019, 512: 148

22 Fattah-Alhosseini A, Keshavarz M K, Molaei M *et al. Metallurgical and Materials Transactions A: Physical Metallurgy and Materials Science*[J], 2018, 49(10): 4966

23 Li Z Y, Cai Z B, Cui X J *et al. Surface and Coatings Technology*[J], 2021, 410: 126949

24 Stojadinović S, Vasilić R, Petković M. *Applied Surface Science*[J], 2013, 265(1): 226

25 Khorasanian M, Dehghan A, Shariat M H. *Surface and Coatings Technology*[J], 2011, 206(6): 1495

26 Kemp R, Sanchez R, Mutch K J *et al. Langmuir*[J], 2010, 26(10): 6967

27 Shokouhfar M, Allahkaram S R. *Surface and Coatings Technology*[J], 2017, 309: 767

28 Sobolev A, Kossenko A, Borodianskiy K. *Materials (Basel, Switzerland)*[J], 2019, 12(23): 3983

29 Shokouhfar M, Allahkaram S R. *Surface and Coatings Technology*[J], 2016, 291: 396

30 Zhang Y, Zhai Y. *RSC Advances*[J], 2016, 6(3): 1750

31 Chen D, Wang R Q, Huang Z Q *et al. Applied Surface Science*[J], 2018, 434: 326

32 Dehnavi V, Shoesmith D W, Luan B L *et al. Materials Chemistry and Physics*[J], 2015, 161: 49

SiO$_2$纳米颗粒/硅酸盐对TC4钛合金微弧氧化膜层性能的影响

孙枫宇[1]，杨　钊[1]，胡　杰[2]，龚云柏[1]，王　平[1]，罗启铭[1]，朱满兰[1]

(1. 西南石油大学 新能源与材料学院，四川 成都 610500)
(2. 低碳智能燃煤发电与超净排放全国重点实验室，江苏 南京 210046)

摘　要：通过向偏铝酸钠基础电解液中加入 SiO$_2$ 纳米颗粒或硅酸钠制备了 TC4 钛合金微弧氧化膜。使用 XRD、SEM、EDS、电化学工作站和摩擦磨损仪检测并分析了添加剂对膜层的影响。结果表明，SiO$_2$ 纳米颗粒和硅酸钠的添加能够显著改善膜层的性能，膜层主要物相为金红石型和锐钛矿型 TiO$_2$、α-Al$_2$O$_3$、γ-Al$_2$O$_3$、Al$_2$TiO$_5$ 与 SiO$_2$。成膜过程中，SiO$_2$ 纳米颗粒和硅酸钠的加入能有效增加膜层的厚度与致密度，同时具有优异物理性能的 SiO$_2$ 纳米颗粒可以直接沉积在放电通道处，大大提高了膜层的耐磨性和耐腐蚀性。其中，添加 SiO$_2$ 纳米颗粒的膜层具有最优异的耐蚀性与耐磨性，腐蚀速率与平均摩擦系数最低分别为 4.095×10^{-5} mm/a 和 0.30。

关键词：微弧氧化；TC4钛合金；膜层；腐蚀；磨损

作者简介：孙枫宇，男，1996年生，硕士生，西南石油大学新能源与材料学院，四川 成都 610500，E-mail：1427153383@qq.com